Scanning Tunneling Microscopy and Theoretical Study of Competitive Reactions in the Dissociative Chemisorption of CCl_4 on Iron Oxide Surfaces

Kwang Taeg Rim,[†] Thomas Müller,[†] Jeffrey P. Fitts,[†,‡] Kaveh Adib,[†,§,||] Nicholas Camillone III,[†,||] Richard M. Osgood,[†,§] Enrique R. Batista,[†,⊥] Richard A. Friesner,[†] S. A. Joyce,[#,@] and George W. Flynn[†,*]

Environmental Molecular Science Institute, Columbia University, New York, New York 10027, Materials Science Program, Department of Applied Physics and Applied Mathematics, Columbia University, New York, New York 10027, and Environmental Molecular Sciences Laboratory, Pacific Northwest National Laboratory, Richland, Washington 99352

Received: July 30, 2003; In Final Form: July 6, 2004

Variable temperature scanning tunneling microscopy (VT STM) and theoretical ab initio computer simulations were used to study dissociative chemisorption and competitive surface chemistry of CCl_4 on an iron-terminated Fe_3O_4 (111) 2×2 surface in an ultrahigh vacuum. The Fe_3O_4 (111) surface was exposed to CCl_4 molecules at 224 K, *slowly* annealed to 500 K (0.2 K/s), and scanned at room temperature. Two different chlorine species were observed only on the iron-terminated Fe_3O_4 (111) 2×2 surface due to chemisorption of CCl_4, one on top of surface-terminating iron atoms (Cl bound to surface irons) and the other at 3-fold oxygen vacancy sites (Cl bound to subsurface irons). The ratio of the number of chlorine species on top sites to the number at 3-fold oxygen vacancy sites is approximately 9:1, which is dramatically different from the 1:10 ratio observed when CCl_4 is dosed at room temperature. The difference in the ratio of these two chlorine species can be explained with a competitive surface reaction picture in which phosgene evolution/surface oxygen atom abstraction, leading to chlorine species at 3-fold oxygen vacancy sites, can only favorably compete with recombination and association reactions, leading to chlorine atoms on top sites, near room temperature. Theoretical calculations were performed that predict an activation barrier of 0.16 eV for the production of phosgene from CCl_4 reacting with the iron-terminated Fe_3O_4 (111) 2×2 surface.

1. Introduction

Iron and oxygen are two of the four most common elements in the Earth's crust, and iron oxides are important minerals in major rock types occurring naturally as the binary iron oxides, such as FeO (wustite), α-Fe_2O_3 (hematite), γ-Fe_2O_3 (maghemite), and Fe_3O_4 (magnetite).[1] Hematite is an important source of iron and the magnetic property of magnetite is useful in high density magnetic recording media applications. Iron oxides have also been used in areas such as heterogeneous catalysis[2,3] and environmental cleanup, e.g., the removal of mobile heavy metal contaminants from aqueous solution,[4] and in the degradation of chlorinated compounds.[5−8] All these applications are related to the surface geometric and electronic structures, surface terminations, defects, and the electrical and magnetic properties of oxides. Thus, a fundamental understanding of the interactions taking place at the interface between molecules and oxide surfaces is of considerable importance.

Since the observation of a chemically reduced surface and superstructure on a single crystal hematite sample with low energy electron diffraction (LEED) and X-ray photoelectron spectroscopy (XPS) in ultrahigh vacuum (UHV) by Ladd et al.,[9] the surface structures and terminations of iron oxides have been the subject of a number of studies. Thornton and co-workers investigated structures and terminations of the selvedge formed at the single crystal α-Fe_2O_3 (0001) surface with LEED and scanning tunneling microscopy (STM) in UHV.[10,11] They reported that a thin film of Fe_3O_4 (111) was formed at the α-Fe_2O_3 (0001) surface and identified it as the reduced surface consisting of two distinctly different terminations. Termination A was identified as $^1/_4$ monolayer of O atoms capping $^3/_4$ monolayer of Fe atoms, whereas termination B consisted of $^1/_2$ monolayer of Fe atoms on top of a close-packed O layer. Weiss and co-workers investigated a magnetite Fe_3O_4 (111) thin film epitaxially grown on a Pt (111) substrate with LEED and STM and found that the polar (111) surface of the magnetite thin film was terminated by $^1/_4$ monolayer of Fe atoms over a close-packed oxygen layer.[12−16] Structural similarities among the three iron oxide phases (wustite, hematite, and magnetite) make it difficult to use STM and LEED measurements alone to unambiguously identify individual phases and determine whether they are iron or oxygen terminated. However, surface structure and surface termination dependent chemistry can help to determine surface terminations.

Previously, we investigated the degradation of CCl_4 and the dissociative chemisorption of Cl_2 on magnetite and biphase selvedges formed on a single crystal α-Fe_2O_3(0001) surface in

* Corresponding author. E-mail address: flynn@chem.columbia.edu. Telephone/Fax: 212-854-4162/212-854-8336.

† Environmental Molecular Science Institute, Columbia University.

‡ Current address: Brookhaven National Laboratory, Environmental Sciences Department, Upton, NY 11973.

§ Materials Science Program, Department of Applied Physics and Applied Mathematics, Columbia University.

|| Current address: Brookhaven National Laboratory, Chemistry Department, Upton, NY 11973.

⊥ Current address: Los Alamos National Laboratory, Theoretical Division, T-12 Mail Stop B268, Los Alamos, NM 87545.

Pacific Northwest National Laboratory.

@ Current address: Los Alamos National Laboratory, Chemistry Division, Mail Stop J567, Los Alamos, NM 87545.

10.1021/jp030937x CCC: $27.50
Published on Web 09/29/2004

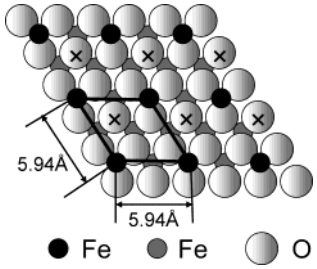

Figure 1. Schematic top view of an iron-terminated Fe_3O_4 (111) 2×2 surface. Large light gray, small black, and small dark gray spheres represent oxygen atoms in the O_c sublayer, Fe_{tet1}, and Fe_{oct1} atoms, respectively (see ref 8). A hexagonal surface unit cell with the dimension of 5.94 Å × 5.94 Å is drawn. Uncapped oxygen atoms at the center of equilateral triangles formed by surface-terminating Fe_{tet1} atoms are marked by ×.

UHV with temperature programmed desorption (TPD),[5] XPS,[7] Auger electron spectroscopy (AES),[6] and STM.[8] These experiments have shown that decomposition of CCl_4 on such a surface follows two basic reaction pathways, one that is favored at low temperature, ultimately producing C_2Cl_4 and recombinant CCl_4, and the other, favored at high temperature, which produces $OCCl_2$. The TPD results indicate that CCl_4 is dissociatively chemisorbed on the magnetite selvedge to produce four desorbing reaction products: recombinative CCl_4, associative C_2Cl_4, $OCCl_2$ following surface oxygen abstraction, and $FeCl_x$ ($x = 1, 2$) following surface iron abstraction. The XPS results suggest that CCl_4 dissociation occurs upon adsorption at temperatures as low as 100 K. Furthermore, the TPD and AES studies indicate that this reaction is not limited to defect sites only, and thus, must occur at regular surface sites. The AES results show no chlorine uptake and hence no reaction on the biphase selvedge, composed of wustite and hematite domains (based on LEED patterns), upon dosing CCl_4 at room temperature.[6] Our STM study on the nominal Fe_3O_4 (111) 2×2 surface identified two distinctly different chlorine species only on the Fe_3O_4 (111) 2×2 iron-terminated surface after dosing CCl_4 at room temperature. Surface termination dependent chemical reactions with CCl_4 and Cl_2 indicate that the Fe_3O_4 (111) 2×2 surface is terminated by $^1/_4$ monolayer of tetrahedrally coordinated iron atoms over a close-packed oxygen layer (see Figure 1). It was also concluded that the nonreactive 1×1 areas of this surface are oxygen-terminated FeO (111) or Fe_3O_4 (111) domains. Surface stoichiometry, termination, reconstruction, and defects are, however, all dependent on surface preparation conditions.

For iron-terminated Fe_3O_4 (111) 2×2 surfaces dosed with CCl_4 at room temperature and flashed to 600 K, two different chlorine species were observed on the surface. These were assigned as chlorine atoms bound on top of surface-terminating lattice irons and chlorine species located at 3-fold oxygen vacancy sites created by surface oxygen abstraction forming phosgene ($OCCl_2$). The number of chlorine atoms at top sites was approximately 10% that of chlorine species at 3-fold oxygen vacancy sites for the surface exposed to CCl_4 at room temperature. The observation that the majority chlorine species is found at 3-fold oxygen vacancy sites after exposing the surface to CCl_4 at room temperature is consistent with TPD results, which show that recombinative and associative reactions (producing CCl_4 and C_2Cl_4) can only dominate over reactions that abstract surface oxygen atoms producing phosgene in the temperature range below ~280 K.

The present study further tests the proposed surface reaction scheme suggested in the TPD study[5] by employing different dosing temperatures from room temperature and scanning at various temperatures. Thus, we use variable temperature STM to investigate competitive surface reactions taking place on the iron-terminated Fe_3O_4 (111) 2×2 surface at temperatures between ~250 and ~400 K after CCl_4 is adsorbed at 224 and 240 K. In section 2, the experimental apparatus and experimental procedures are presented. In section 3 computational methods, utilized for the ab initio computer simulations employed to determine the activation barrier for phosgene production, are described. The crystal structure of magnetite is briefly described in section 4.1, and previous TPD results and room temperature STM results are reviewed in section 4.2. In section 4.3, the results of the present variable temperature STM experiments and theoretical calculations are discussed in the context of the competitive surface reactions and the previous TPD results.

2. Experimental Section

The experiments were performed in an ultrahigh vacuum (UHV) chamber with a base pressure of 3×10^{-10} Torr. The chamber is equipped with an ion gun, rear view LEED optics (Princeton Research Instruments), a quadrupole mass spectrometer, and a commercial VT STM (Omicron GmbH) capable of scanning at temperatures ranging from 25 to 1500 K.

A natural single crystal α-Fe_2O_3 sample was sliced and polished to a mirror finish within ±0.5° of the (0001) plane (Commercial Crystal Laboratories, Inc.) as confirmed by Laue X-ray diffraction. Prior to insertion into the UHV chamber via a turbo-pumped loadlock, the 6.5 mm × 6.5 mm × 2 mm α-Fe_2O_3 sample was rinsed with methanol, blown with dry nitrogen and mounted onto a resistive heating sample holder with a solid-state Pyrolytic Boron Nitride (PBN) heating element.

The crystal was cleaned in situ by repeated cycles of Ar^+ ion sputtering for 15 min at 2 kV (~3 μA sample current) followed by annealing in a vacuum (using the PBN heater) for 15 min at $T = 860$ K, as measured by an infrared pyrometer (Omega Engineering, Inc. OSP1300). Sample surface preparation, orderliness, and cleanliness were assessed qualitatively on the basis of the sharpness of LEED patterns. A sharp hexagonal 2×2 LEED pattern, obtained following the sample preparation procedures described above and shown in Figure 2, is consistent with a bulk-terminated Fe_3O_4 (111) surface. Upon obtaining such a LEED pattern, the sample was transferred to the STM sample stage and imaged at room temperature. Once well-resolved images were obtained, the sample was cooled to ~200 K and exposed to 0.3 langmuir of CCl_4 by backfilling the chamber. After dosing with CCl_4, the sample surface was scanned in two different ways. First, the sample temperature was slowly ramped from ~200 to 500 K (to remove all organic compounds left behind on the surface after dissociative chemisorption of CCl_4) and then lowered to room temperature, and then the sample was scanned again at room temperature. Second, after dosing at ~200 K, the sample temperature was raised to 260 K and the sample was scanned at 260 K. After scanning at 260 K, the sample temperature was further raised to 280 K where the sample was again scanned. In both cases, representative images acquired before and after dosing with CCl_4 were compared to identify reaction products, surface terminations, and structure−reactivity/termination-dependent-reactivity relationships of the majority and minority phases on the surface. The identification of reaction products and surface terminations was also aided by additional information from *Scanning Tunneling Spectroscopy* (STS) on single surface points where I/V curves were obtained over surface atoms and adsorbates.

Argon (99.9999%, H_2O residue < 1 ppm) and oxygen (99.998%, H_2O residue < 1 ppm) gases were purchased from

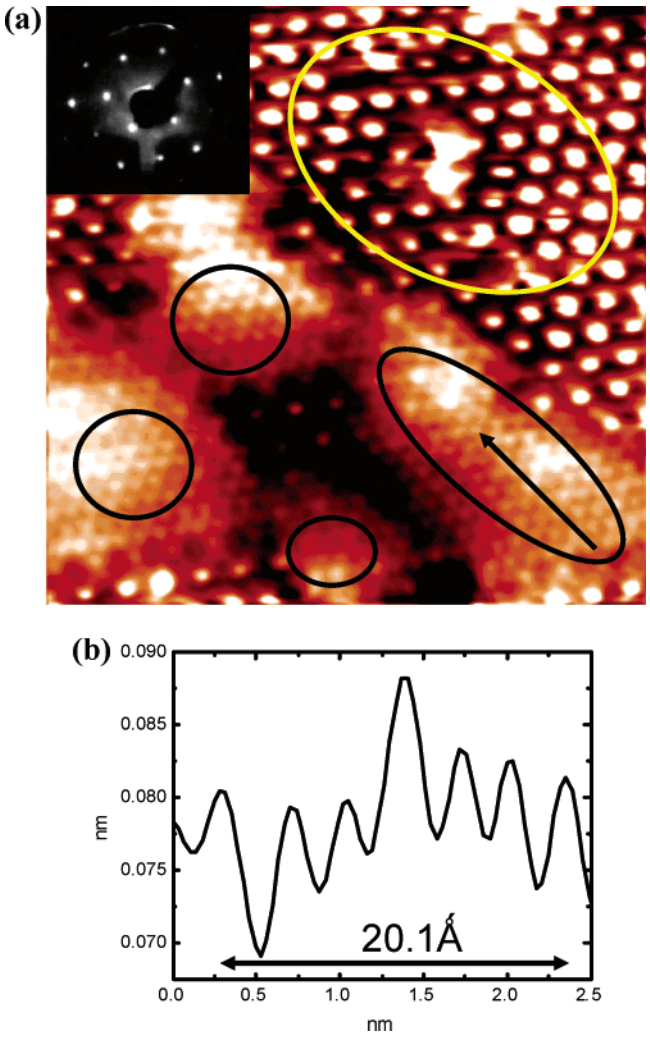

Figure 2. STM image of the pristine Fe_3O_4 (111) surface before dosing with CCl_4. The STM image in (a), 12 × 12 nm^2, shows the coexistence of two distinct surface phases. The majority phase is Fe-terminated Fe_3O_4 (111) 2 × 2 marked by a large yellow circle, and the minority phase is O-terminated FeO (111)/Fe_3O_4 (111) 1 × 1 marked by black circles. The line profile in (b) along the arrow of image (a) reveals that the spacing between bright protrusions is approximately 3 Å, the unit cell dimension of a close-packed oxygen layer. A LEED pattern (at 81 eV) shown in the upper left corner of the image is consistent with an Fe_3O_4 (111) 2 × 2 surface structure.

Matheson Tri-Gas Inc. and used without further purification. Carbon tetrachloride (99.9+%, H_2O residue < 0.01%) was obtained from Aldrich and purified by several freeze−pump−thaw cycles prior to backfilling the UHV chamber. Tungsten tips were electrochemically etched in 3 N NaOH solution and degassed by heating to 473 K in the UHV chamber. All STM images were recorded in constant current mode. Bright features in the images taken with the surface biased positive correspond to empty states of surface atoms and adsorbates.

After each STM investigation exposing the surface to CCl_4, the sample surface was sputtered and annealed at 860 K in a partial pressure of 1.0×10^{-6} Torr O_2 followed by annealing in a vacuum before new experiments were begun. This oxidation procedure removes adsorbates on the surface after each chemistry study with CCl_4. Multiple cycles of sample preparation (sputtering and annealing in a vacuum) can cause enough oxygen deficiency in the bulk to make the surface unstable. Unstable Fe_3O_4 surface films tend to reconstruct, forming a more stable structure (e.g., biphase reconstruction). Annealing in O_2 provides sufficient oxygen to produce a stable Fe_3O_4 (111) surface and removes surface contaminants effectively. When the sample was exposed to air, it was also annealed as above in O_2 to remove contaminants.

3. Computational Methods

The magnetite surface was studied via the embedded cluster method presented in a previous paper[17] and summarized in the present section. The structure of a magnetite surface terminated with $^1/_4$ monolayer of iron atoms (see details of the crystal structure in section 4.1) was obtained by standard procedures for surface calculations. First we obtained the bulk structure of the crystal for the desired level of theory and then a slab-type calculation was performed to allow for surface relaxations.

The bulk structure was optimized using density functional theory (DFT) with periodic boundary conditions. For this calculation the Vienna Ab initio Simulation Program (VASP)[18−21] was used. For the exchange−correlation functional, the gradient corrected functional by Perdew and Wang[22,23] was employed. The core electrons were represented by ultrasoft Vanderbilt-type pseudo-potentials,[24] and only the valence electrons were treated explicitly as Kohn−Sham orbitals expanded in a basis of spin-polarized plane-wave Bloch functions. The bulk unit cell contained 18 iron and 24 oxygen atoms with a volume of 512.2 Å^3. The unit cell has hexagonal symmetry with a length of 14.54 Å along the [111] direction and the unit vectors in the (111) plane were 5.94 Å long and form an angle of 60°. Because the unit cell was already rather large, only the Γ-point was used in *k*-space. During the bulk optimization, all the atoms as well as the dimensions of the simulation box were allowed to relax. The relaxed lattice structure for the level of theory under consideration was 2% shorter along the [111] axis and 1% longer in the perpendicular plane compared with the experimental bulk structure.

After the bulk structure was obtained, the relaxation of the surface was obtained from a slab-type calculation. The box size along the [001] plane was augmented with a 10 Å vacuum gap, leaving a $^1/_4$ monolayer of iron atoms exposed. The top layers experienced significant relaxation. The interlayer relaxations between the Fe−O−Fe−O−Fe−Fe−Fe layers along the [111] direction were −37%, −21%, +7%, −4%, −2%, and 1%, respectively. Five layers below the surface into the bulk no significant atomic relaxations with respect to the bulk structure were observed. We note that the interlayer relaxations in our calculated model surface qualitatively agree with the result that Ritter et al. obtained using a full dynamical low energy electron diffraction (LEED) intensity analysis.[14]

From this optimized surface, clusters were selected with seven layers along the [111] direction that contained the binding site under study away from the edges of the cluster. The clusters were chosen to satisfy the stoichiometry of magnetite (3 parts iron and 4 parts oxygen). The clusters used contained 42 atoms with a surface area of 70 Å^2. The clusters were embedded in a set of point charges placed at the lattice positions up to a radius of 12 Å. The value of the charges was chosen according to a self-consistent procedure.[17] The electronic structure of the cluster was calculated via DFT using the hybrid functional B3LYP[25] and the Jaguar v. 4.1 suite[26] of ab initio quantum chemistry programs. For the iron atoms we used the LACVP basis set with effective core potential[27,28] whereas 6-31G[29] was used for the oxygen atoms. This choice of basis set was shown to work well in a previous publication.[17]

The binding energy of adsorbates was taken to be the energy difference ΔE, defined as $\Delta E = E(\text{surface} + \text{molecule}) - [E(\text{surface}) + E(\text{molecule})]$. The energy $E(\text{surface} + \text{molecule})$

is the total energy of the system composed of the surface cluster and the adsorbed molecule at the binding position. *E*(surface) is the total energy of the surface cluster and *E*(molecule) is the energy of the free adsorbate molecule. Only the relaxations of the nearest neighbors to the adsorption site were included in the calculation.

4. Results and Discussion

4.1. Crystal Structure and Surface Terminations of Fe_3O_4. Single crystal magnetite has the inverse spinel structure in which oxygen atoms form a close-packed face-centered cubic sublattice with iron atoms located at interstices between oxygen sublayers. There are two different sites that iron atoms can occupy. Tetrahedral (A) sites are occupied by Fe^{3+} ions and octahedral (B) sites are occupied half by Fe^{3+} ions and half by Fe^{2+} ions. The cubic unit cell can be denoted as $(Fe^{3+})_8{}^{tet}(Fe^{2+}Fe^{3+})_8{}^{oct}O_{32}$ with a lattice constant of 8.396 Å. Above the Verwey transition temperature (120 K),[30] the high electrical conductivity of the crystal is due to electron hopping within the octahedral B sublattice. Electron hopping stops and the crystal becomes insulating below the Verwey transition temperature, where the sample surface can no longer be imaged with a STM. Along the [111] direction, two types of iron sublayers, one with all octahedrally coordinated Fe ions (Fe^{2+}, Fe^{3+}) and the other with octahedrally and tetrahedrally coordinated Fe ions (Fe^{3+}) alternate between cubic close-packed oxygen sublayers. The stacking sequence along the [111] direction can be schematically represented by $Fe_{tet1}-O_C-Fe_{oct1}-O_B-Fe_{tet2}-Fe_{oct2}-Fe_{tet1}-O_A$ and is shown in Figure 1 of ref 8. Here, subscripts tet1 and tet2 refer to 4-fold coordinated Fe layers, and oct1 and oct2 correspond to Fe layers where the iron atoms are 6-fold coordinated to O atoms. O_A, O_B, and O_C correspond to cubic close-packed O sublayers. The height of the repeating unit along the [111] direction is ~4.8 Å, and the unit cell dimension in the close-packed O sublayer is 2.96 Å.

Figure 1 shows the schematic top view of an Fe_{tet1}-terminated surface in the unreconstructed Fe_3O_4 (111) bulk structure.[8,14] This surface-terminating Fe_{tet1} layer constitutes $^1/_4$ monolayer of iron atoms over a close-packed O layer, forming a 2×2 surface structure with the hexagonal surface unit cell dimension of 5.94×5.94 Å^2. Each Fe_{tet1} atom has one dangling bond normal to the surface and oxygen atoms uncoordinated with surface-terminating Fe_{tet1} are denoted by $\times$. Each surface unit cell has one Fe_{tet1} atom and one uncoordinated oxygen atom ($\times$).

4.2. Competitive Surface Reactions (TPD and Room Temperature STM). In a previous publication we reported temperature programmed desorption (TPD) studies characterizing the surface chemistry upon dosing CCl_4 at 100 K on a nominal Fe_3O_4 (111) surface, which was prepared similarly to the present sample as confirmed by the 2×2 LEED pattern.[5] TPD results exhibit six separate desorption features involving four desorbing species, CCl_4, $OCCl_2$ (phosgene), C_2Cl_4 (tetrachloroethylene), and $FeCl_x$ ($x = 1$, 2, iron chloride). The first two peaks in the CCl_4 spectrum correspond to multilayer and monolayer desorption of molecular CCl_4 at 167 and 206 K, respectively. Monolayer desorption of CCl_4 molecules indicates physisorption on the unreactive sites of the nominal Fe_3O_4(111) 2×2 surface, which is described by

$$CCl_4(g) \xrightarrow[100\ K]{} CCl_4(ad) \xrightarrow{\Delta} CCl_4(g) \qquad (1)$$

Dissociative chemisorption of CCl_4 also takes place on the surface below 250 K and produces chlorocarbon fragments and chlorine atoms on the surface. As the temperature is ramped up, four different chlorinated compounds desorb: CCl_4 by recombinative desorption, C_2Cl_4 by associative desorption, $OCCl_2$ by surface oxygen abstraction, and $FeCl_x$ by surface iron abstraction. The recombinative desorption of CCl_4 and the associative desorption of C_2Cl_4 take place in the temperature range from 250 to 300 K and 250 to 380 K, respectively, whereas phosgene desorbs between 280 and 400 K. The observation that the onset temperature of $OCCl_2$ desorption coincides with the peak temperature of recombinative CCl_4 and associative C_2Cl_4 desorption suggests that competitive reaction occurs among three different reaction pathways described by

$$CCl_4(g) \xrightarrow[100\ K]{} CCl_2(ad) + 2Cl(ad) \xrightarrow{\Delta} CCl_4(g) \qquad (2a)$$

$$CCl_2(ad) \xrightarrow{\Delta} {}^1/_2C_2Cl_4(g) \qquad (2b)$$

$$CCl_2(ad) + O(lattice) \xrightarrow{\Delta} OCCl_2(g) \qquad (2c)$$

Approximately 75% of the dosed CCl_4 molecules are dissociatively adsorbed on the surface, leading to the competitive reaction chemistry described by eq 2a−c. The remaining 25% of the CCl_4 molecules are physisorbed on the unreactive area of the surface, where desorption is described by eq 1.[5] This conclusion is consistent with STM images of the surface showing a nominal iron-terminated Fe_3O_4 (111) 2×2 surface coexisting with other surface phases, which have different surface structures or terminations (see below).

The STM image of a pristine oxide surface in Figure 2a, recorded at room temperature, shows the coexistence of two distinct surface structures. The area marked by the yellow circle exhibits the Fe-terminated Fe_3O_4 (111) 2×2 surface with a 6 Å surface unit cell constant. The areas marked by black circles show the O-terminated FeO (111)/Fe_3O_4 (111) 1×1 surface where the spacing between close-packed oxygen atoms is approximately 3 Å, as shown in the line profile in Figure 2b taken along the arrow in Figure 2a. Although STS spectroscopy of the Fe-terminated 2×2 surface shows both filled and empty states, the O-terminated 1×1 surface reveals only empty states (see Figure 6 of ref 8 for *I*(*V*) curves). The LEED pattern included as an inset within Figure 2a reveals the nominal overall surface structure of Fe_3O_4 (111) 2×2. Approximately 75%−85% of this surface is attributable to the reactive, iron-terminated Fe_3O_4 (111) 2×2 surface whereas the remaining 15%−25% is the unreactive oxygen-terminated surface in agreement with previous TPD and STM studies.[5,8]

In a previous STM study,[8] the nominal Fe_3O_4 (111) 2×2 surface (see Figures 5a and 7a of ref 8) was prepared and exposed to 0.1 langmuir of CCl_4 molecules at room temperature. The sample was then flashed to 600 K and cooled to room temperature in order to image the chlorinated iron oxide surface without chlorocarbon species. Two different chlorine species, located on the top of lattice iron atoms and at 3-fold oxygen vacancy sites, were identified. Approximately 90% of the chlorine species on the surface were found to be located at 3-fold oxygen vacancy sites, which appear brighter, larger, and less circular (~6 Å wide, 1.2 Å high) than top site chlorine species (see Figure 8 of ref 8). This observation suggests that a large fraction of dissociatively adsorbed CCl_4 reacts with the surface at room temperature to produce phosgene and corresponding oxygen atom vacancy sites. However, the TPD results point to a smaller fraction of dissociative adsorption, leading to phosgene production when CCl_4 is dosed at temperatures below 280 K, the onset temperature for phosgene production. Instead, the TPD

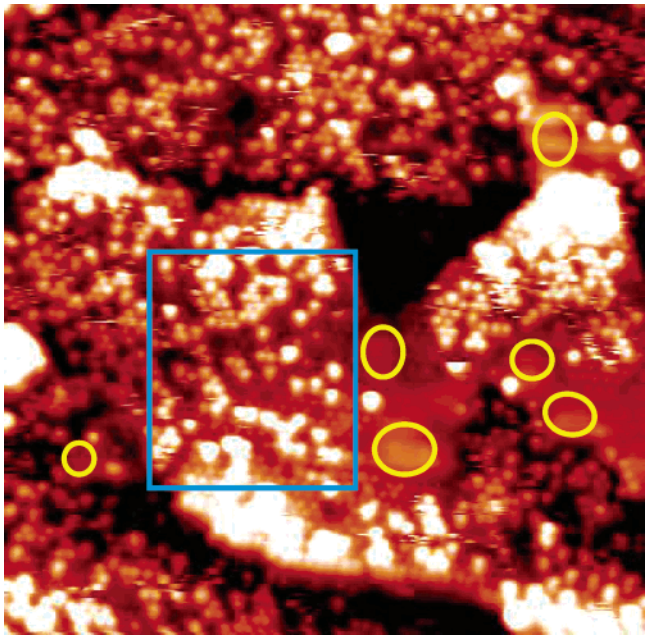

Figure 3. STM image of the Fe_3O_4 (111) surface after dosing with CCl_4 at 224 K. This STM image, 35 × 35 nm^2 at $V = 1.5$ V and $I = 0.7$ nA, was acquired after the surface was exposed to 0.3 langmuir of CCl_4 at 224 K, annealed *slowly* up to 500 K, and cooled to room temperature. Chlorine species (bright features) are observed on the Fe-terminated Fe_3O_4 (111) 2 × 2 surface, but not on the O-terminated FeO (111)/Fe_3O_4 (111) 1 × 1 surface areas marked by the yellow circles. The area indicated by the blue rectangle is enlarged in Figure 4 to show chlorine species more clearly.

data indicate that at this lower temperature a relatively larger fraction of the dissociatively adsorbed CCl_4 is expected to be desorbed via the recombinative and associative reactions that produce CCl_4 and C_2Cl_4 without removing surface oxygen atoms.

4.3. Competitive Surface Reactions (Variable Temperature STM and Theoretical Studies). To further investigate the competitive surface chemical reactions described by eq 2a−c, the nominal magnetite surface was exposed to 0.3 langmuir of CCl_4 at 224 K and the temperature was *slowly* ramped up to 500 K (∼0.2 K/s) and cooled to room temperature to image the surface. The image in Figure 3 was obtained at room temperature after the procedure described above. Bright features on the surface in the image, which are chlorine species remaining from the dissociative chemisorption of CCl_4,[8] cover approximately 30% of the whole surface. These bright features were found only on the Fe-terminated Fe_3O_4 (111) 2 × 2 areas in this study and in a previous investigation.[8] Topographical or electronic structure changes due to adsorbates on O-terminated FeO (111)/Fe_3O_4 (111) 1 × 1 areas marked by yellow circles in Figure 3, typically characterized by additional bright features or dark depressions in the STM images, were not observed. Thus we conclude that any chlorine species, which were found on Fe-terminated areas, were not present on any O-terminated regions. This is also consistent with the picture presented by STS spectroscopy in which only Fe atom sites can serve as a source of low to moderate energy electrons, as observed in our previous STM studies.[8] In an earlier AES study,[6] chlorine species were also observed on the Fe_3O_4 (111) 2 × 2 surface after dosing CCl_4 at room temperature; however no chlorine species were detected on the biphase superstructure surface, consisting of FeO (111) and α-Fe_2O_3 (0001) domains.

Parts a and b of Figure 4 show two consecutive images of the area marked by the blue rectangle in Figure 3, i.e., a Fe_3O_4 (111) 2 × 2 area, separated in time by approximately 5 min. Two different chlorine species are clearly observed. The majority chlorine species, marked by yellow and black circles, are located on top of surface-terminating iron atoms. These atoms appear to aggregate, forming triangles (small yellow circles in Figure 4a,b), 2D clusters (the large yellow circle in Figure 4b), or linear chains (the black circle in Figure 4b). This aggregation is attributable to the weak binding of the top site majority chlorine species to surface iron atoms, resulting in mobility at room temperature. This point is further discussed below in the context of the theoretical calculations of binding energies of Cl on iron atoms. The minority chlorine species, marked by white circles, are positioned in the centers of equilateral triangles formed by surface iron atoms, which correspond to 3-fold oxygen vacancy

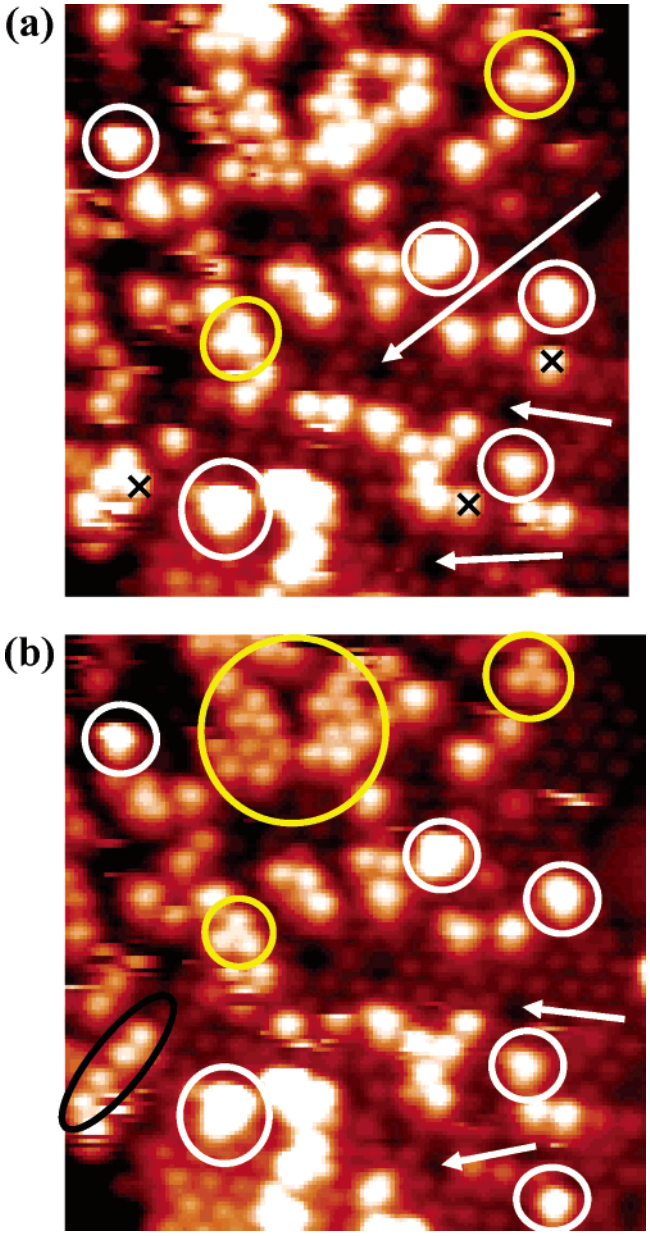

Figure 4. Enlarged STM image of the area indicated in Figure 3. Two consecutive images of the area indicated in Figure 3 are shown in (a) and (b), which are separated in time by approximately 5 min. Two different chlorine species are clearly identified: one on top of surface-terminating Fe atoms marked by yellow circles and the other at 3-fold oxygen vacancy sites (TFOVS) marked by white circles. Top site chlorine species marked by × in (a) disappear in (b), which indicates they are mobile at room temperature. Chlorine species are not observed at the iron defect sites indicated by the white arrows in (a) and (b).

sites created through oxygen abstraction to form phosgene ($OCCl_2$). Chlorine atoms from CCl_4 dissociation on the surface fill these oxygen vacancies to form the minority chlorine species.

An analysis of the statistical distribution of these two distinct chlorine moieties, obtained by counting individual bright features in well-resolved images over a wide area, shows that the number of minority chlorine species is 10−15% of the majority top site chlorine atoms. In contrast, when this same surface is exposed to CCl_4 at room temperature, flashed to 600 K, and scanned at room temperature, about 90% of the chlorine species are located at 3-fold oxygen vacancy sites (see Figure 8 of ref 8). The critical difference between the previous and present experiments is the temperature at which the sample surface was first exposed to CCl_4 molecules. When CCl_4 is dosed on the sample surface at all temperatures investigated, dissociation occurs and surface chemistry follows, as described by eq 2a−c. However, CCl_4 dosing at low temperature (224 K) favors recombinative CCl_4 desorption and associative C_2Cl_4 desorption reaction channels (eq 2a,b), which open up at temperatures as low as 250 K.[5] The surface reaction channel producing phosgene (described in eq 2c) does not open until 280 K.[5] Thus, dosing at 300 K allows abstraction of surface oxygen atoms (likely the uncapped ones marked by × in Figure 1) to compete with recombination and association processes that evidently have lower reaction barriers. In the present experiments, where CCl_4 molecules are dosed on the sample surface at 224 K and the temperature is *slowly* increased to 500 K (∼0.2 K/s), we do not expect many oxygen vacancies due to oxygen abstraction because recombinative and associative desorption channels dominate. This nicely explains the result that the majority chlorine species appearing at 3-fold oxygen vacancy sites when CCl_4 is dosed at room temperature becomes the minority chlorine species upon dosing CCl_4 at 224 K.

The activation energy for phosgene desorption was calculated, using a 42-atom cluster, as described in section 3. A CCl_2 radical was placed close to an uncapped surface oxygen atom, marked by × in Figure 1, and the geometry of the whole molecule was optimized by energy minimization. The optimal position of a phosgene molecule was located at the point where the oxygen atom was 0.1 Å below the surface iron atoms and the O−C bond length was 1.22 Å with CCl_2 pointing out of the surface. The potential energy curve for the abstraction of a phosgene molecule was mapped by gradually displacing the molecule. At each step, the vertical coordinate of the oxygen atom with respect to the surface was varied whereas all the other degrees of freedom of the molecule were optimized by energy minimization. The potential energy of the system as a function of the vertical displacement of a phosgene molecule is shown in Figure 5. The *z* coordinate corresponds to the position of the oxygen atom (×) in Figure 1 with respect to the surface-terminating iron layer. An activation energy barrier of 0.16 eV is found when the molecule moves 0.20 Å vertically over the (111) surface, after which point the molecule is repelled away. This theoretical calculation indicates that uncapped surface oxygen atoms (×) are not bonded strongly with subsurface iron atoms and that CCl_2 can readily abstract these atoms once phosgene is formed. Thus, phosgene likely forms around ∼280 K and starts desorbing right after formation.

The white arrows in Figure 4a,b indicate surface iron atom defect sites, and the images show that chlorine atoms are not bonded to these subsurface oxygen atom sites. Cl atoms have not been observed at step edges either. These observations strongly suggest that surface reaction with CCl_4 occurs on regular terraces but not at defect sites. Note that the top site

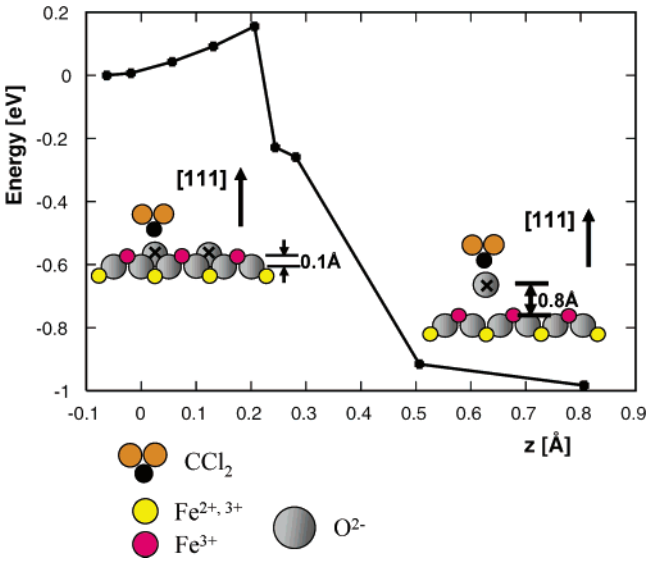

Figure 5. Activation energy for desorption of an $OCCl_2$ molecule from the Fe_3O_4 (111) surface. Potential energy of the system is shown as an $OCCl_2$ molecule is moved vertically from the Fe_3O_4 (111) surface. The *z* coordinate corresponds to the vertical position of the oxygen atom (×) (see Figure 1) from the surface-terminating iron layer. The activation energy is approximately 0.16 eV at $z = 0.2$Å. The figure on the left (right) shows the formation (desorption) of a phosgene molecule. Oxygen atoms (large gray balls) are 0.1 Å below the surface-terminating iron layer (small red balls) when a phosgene molecule is formed. Small yellow balls are octahedrally coordinated subsurface iron atoms. Uncapped oxygen atoms (×) are in the same plane with the capped oxygen atoms (see Figure 1).

chlorine atoms marked by × in Figure 4a disappear in Figure 4b. This implies that top site chlorine atoms are weakly bound to surface iron atoms and mobile at room temperature. This observation is consistent with the results of theoretical calculations that predict the binding energy of a chlorine atom at a 3-fold oxygen vacancy site is 1.5 eV larger than that at a top site. The larger binding energy at a 3-fold oxygen vacancy site is attributed to the presence of three "undercoordinated" iron atoms exposed after oxygen atom removal. In the experiments described above, where the sample was annealed at 500 K before scanning at room temperature, TPD studies show clearly that no carbon containing species remain on the surface and adsorbates observed with STM can be readily assigned as Cl atoms.[5]

We have also dosed 0.3 langmuir of CCl_4 on an iron oxide surface at 240 K followed by scanning at 260 and 280 K without annealing the surface up to 500 K. The STM topographs obtained following this procedure are shown in Figure 6a,b. Images taken at both temperatures reveal that no bright features are found on oxygen-terminated FeO (111)/Fe_3O_4 (111) 1 × 1 areas. Small bright spots, which are very similar to features assigned as chlorine atoms for samples annealed to 500 K, appear on top of surface iron atoms. Big bright spots, which are similar in shape, size, and location to features assigned as chlorine atoms at 3-fold oxygen vacancy sites for samples annealed to 500 K, also appear in the center of equilateral triangles formed by surface iron atoms (see Figure 4a,b as well as Figure 8 of ref 8). The number of top site species are again dominant over those found at 3-fold oxygen vacancy sites in the iron-terminated Fe_3O_4 (111) 2 × 2 areas. Very few bright features are observed at 3-fold oxygen vacancy sites in Figure 6a. These observations are in agreement with the picture of competitive surface reactions occurring among reaction intermediates described above because the phosgene producing

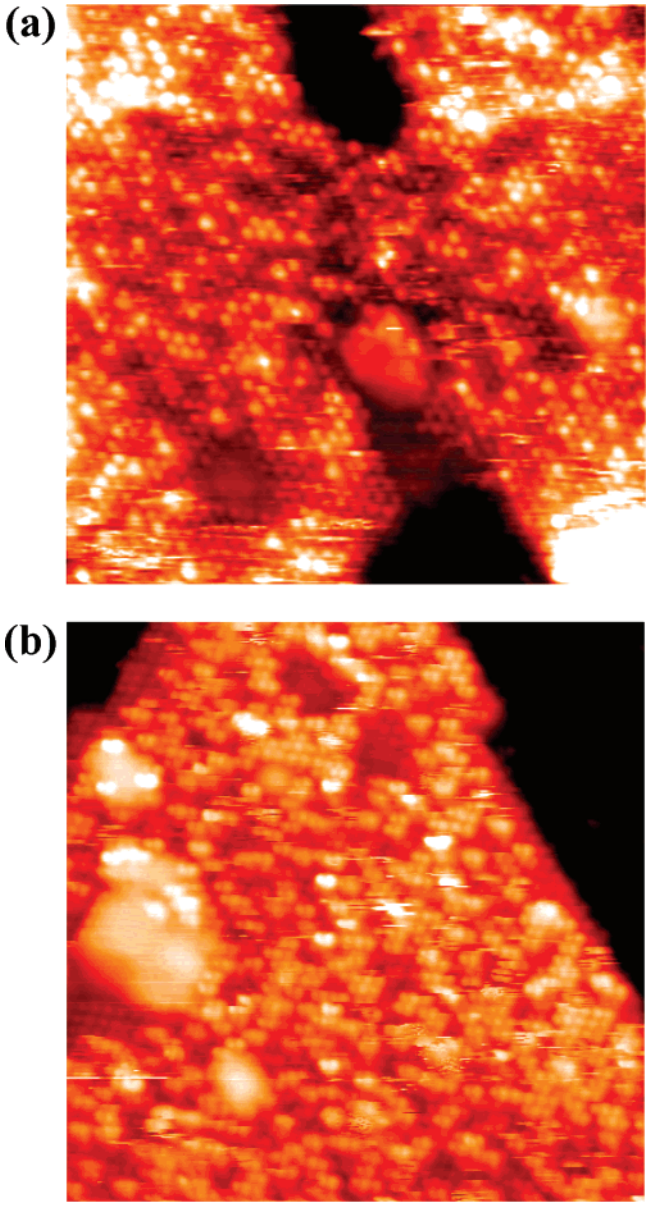

Figure 6. STM image of the Fe_3O_4 (111) surface after dosing with CCl_4 at 240 K. The image in (a), 35 × 35 nm^2, obtained at 260 K after dosing CCl_4 at 240 K reveals that chlorines are found only on the Fe-terminated Fe_3O_4 (111) 2 × 2 surface. Very few chlorine species are observed at 3-fold oxygen vacancy sites (TFOVS). The image in (b), 35 × 35 nm^2, was obtained at 280 K after recording the image in (a).

channel has its onset near 280 K. Although the possibility that some carbon containing species may remain on the surface cannot be ruled out in these "nonannealed" experiments, both the similarity of the STM images to those observed in the annealed case and the TPD results (showing that the onset of desorption for organic species begins at 250 K) suggest that the surface adsorbates in this case are also dominated by Cl atoms. The image in Figure 6b acquired at 280 K also reveals that top site chlorine species are more aggregated than at 260 K, but no appreciable change in the number of chlorine species at 3-fold oxygen vacancy sites is observed. Thus the results of these variable temperature STM studies at 260 and 280 K suggest that the dissociative chemisorption of CCl_4 does indeed take place on the iron-terminated Fe_3O_4 (111) 2 × 2 surface through competitive surface reactions at these temperatures, in agreement with the results of the previous TPD study.

5. Summary and Conclusion

The degradation and competitive reaction of CCl_4 molecules on the reduced sample surface of a single crystal α-Fe_2O_3 (0001) were studied with variable temperature scanning tunneling microscopy. STM images at room temperature were obtained after the sample surface was exposed to CCl_4 molecules at 224 K and annealed *slowly* up to 500 K (~0.2 K/s). Images reveal that chlorine species are bonded only on iron-terminated Fe_3O_4 (111) 2 × 2 areas not on oxygen-terminated FeO (111)/Fe_3O_4 (111) 1 × 1 areas. Two different chlorine species, one set on top of surface-terminating iron atoms and the other set at 3-fold oxygen vacancy sites, were observed. Ninety percent of the chlorine species are found at top sites. This contrasts sharply with the results observed when CCl_4 was dosed on the reduced sample surface at room temperature, flashed to 600 K, followed by surface scanning at room temperature.[8] These observations have been explained with a competitive surface reaction picture in which phosgene production/oxygen atom abstraction can only compete favorably with recombination and association near or above room temperature. Theoretical calculations predict that uncapped surface oxygen atoms are relatively weakly bound to subsurface iron atoms and easily abstracted by a CCl_2 intermediate to form phosgene. STM images show that only top site chlorine atoms are mobile at room temperature, which is qualitatively consistent with theoretical calculations that chlorine species at 3-fold oxygen vacancy sites are 1.5 eV more strongly bound than top site chlorine atoms.

Acknowledgment. This work was supported by grants from the National Science Foundation (CHE-00-95649 and CHE-03-52582) and jointly by the National Science Foundation and the U.S. Department of Energy through a grant to the Environmental Molecular Science Institute at Columbia University (NSF CHE-98-10367). S.A.J. acknowledges the support of the Environmental Molecular Sciences Laboratory, a national scientific user facility sponsored by the Department of Energy's Office of Biological and Environmental Research and located at Pacific Northwest National Laboratory.

References and Notes

(1) Schwertman, U.; Cornell, R. M. *Iron Oxides in the Laboratory: Preparation and Characterization*; VCH: Weinheim, 2000.
(2) Ranke, W.; Weiss, W. *Surf. Sci.* **1998**, *414*, 236.
(3) Street, S. C.; Xu, C.; Goodman, D. W. *Annu. Rev. Phys. Chem.* **1997**, *48*, 43.
(4) Qiu, S. R.; Lai, H.-F.; Roberson, M. J.; Hunt, M. L.; Amrhein, C.; Giancarlo, L. C.; Flynn, G. W.; Yarmoff, J. A. *Langmuir* **2000,** *16*, 2230.
(5) Adib, K.; Camillone, N., III; Fitts, J. P.; Rim, K. T.; Flynn, G. W.; Joyce, S. A.; Osgood, R. M., Jr. *Surf. Sci.* **2002**, *497*, 127.
(6) Camillone, N., III; Adib, K.; Fitts, J. P.; Rim, K. T.; Flynn, G. W.; Joyce, S. A.; Osgood, R. M., Jr. *Surf. Sci.* **2002**, *511*, 267.
(7) Adib, K.; Mullins, D. R.; Totir, G.; Camillone, N., III; Fitts, J. P.; Rim, K. T.; Flynn, G. W.; Osgood, R. M., Jr. *Surf. Sci.* **2003**, *524*, 113.
(8) Rim, K. T.; Fitts, J. P.; Müller, T.; Adib, K.; Camillone, N., III; Osgood, R. M., Jr.; Joyce, S. A.; Flynn, G. W. *Surf. Sci.* **2003**, *541*, 59.
(9) Ladd, R. J.; Henrich, V. E. *Surf. Sci.* **1988**, *193*, 81.
(10) Condon, N. G.; Murray, P. W.; Leibsle, F. M.; Thornton, G.; Lennie, A. R.; Vaughan, D. J. *Surf. Sci. Lett.* **1994**, *310*, L609.
(11) Condon, N. G.; Leibsle, F. M.; Lennie, A. R.; Murray, P. W.; Parker, T. M.; Vaughan, D. J.; Thornton, G. *Surf. Sci.* **1998**, *397*, 278.
(12) Weiss, W.; Barbieri, A.; Van Hove, M. A.; Somorjai G. A. *Phys. Rev. Lett.* **1993**, *71*, 1848.
(13) Barbieri, A.; Weiss, W.; Van Hove, M. A.; Somorjai G. A. *Surf. Sci.* **1994**, *302*, 259.
(14) Ritter, M.; Weiss, W. *Surf. Sci.* **1999**, *432*, 81.
(15) Shaikhutdinov, S. K.; Joseph, Y.; Kuhrs, C.; Ranke, W.; Weiss, W. *Faraday Discuss.* **1999**, *114*, 363.
(16) Shaikhutdinov, S. K.; Ritter, M.; Wang, X.-G.; Over, H.; Weiss, W. *Phys. Rev. B* **1999**, *60*, 11062.
(17) Batista, E. R.; Friesner, R. A. *J. Phys. Chem. B* **2002**, *106*, 8136.
(18) Kresse, G.; Hafner, J. *Phys. Rev. B* **1993**, *47*, 558.

(19) Kresse, G.; Hafner, J. *Phys. Rev. B* **1994**, *49*, 14251.
(20) Kresse, G.; Furthmüller, J. *Phys. Rev. B* **1996**, *54*, 11169.
(21) Kresse, G.; Furthmüller, J. *Comput. Mater. Sci.* **1996**, *6*, 15.
(22) Perdew, J. P. Unified theory of exchange and correlation beyond the local density approximation. *Electronic Structure of Solids '91* **1991**.
(23) Perdew, J. P.; Wang, Y. *Phys. Rev. B* **1992**, *45*, 13244.
(24) Kresse, G.; Hafner, J. *Phys.: Condens. Matter* **1994**, *6*, 8245.
(25) Becke, A. D. *J. Chem. Phys*. **1993**, *98*, 1372.
(26) *Jaguar v. 4.1;* Schrodinger, Inc.: Portland, OR, 2000.
(27) Hay, P.; Wadt, W. *J. Chem. Phys.* **1985**, *82*, 270.
(28) Wadt, W.; Hay, P. *J. Chem. Phys.* **1985**, *82*, 284.
(29) Hehre, W.; Ditchfield, R.; Pople, J. *J. Chem. Phys.* **1972**, *56*, 2257.
(30) Zhang, Z.; Satpathy, S. *Phys. Rev. B* **1991**, *44*, 13319.